Available online at www.sciencedirect.com
SCIENCE DIRECT®
International Journal of Heat and Mass Transfer 47 (2004) 1433–1444
International Journal of HEAT and MASS TRANSFER
www.elsevier.com/locate/ijhmt

Velocity and temperature measurements in an axisymmetric turbulent jet with cloud-like off-source heating

Amit Agrawal [a], K.R. Sreenivas [b,1], Ajay K. Prasad [a,*]

[a] Department of Mechanical Engineering, University of Delaware, 126 Spencer Lab, Newark, DE 19716, USA
[b] Engineering Mechanics Unit, Jawaharlal Nehru Center for Advanced Scientific Research, Bangalore 560064, India

Received 4 June 2002; received in revised form 18 September 2003

Abstract

A laboratory analogue consisting of a volumetrically heated turbulent axisymmetric jet was created to study the effect of latent heat release on entrainment in cumulus clouds. The jet fluid was selectively heated in the experiment to simulate condensation heat release in clouds. Whole-field velocity and temperature measurements were conducted in the axial plane of the jet in the heat injection zone (HIZ). Results are presented for varying Reynolds number and non-dimensional heat injection rate. We find that the entire HIZ can be divided into three sub-zones with sharp differences in flow properties based primarily on the nature of the cross-stream velocity profile. The cross-stream velocity profile shows a gradual disappearance of the region of outflow near the jet axis which can be attributed to the acceleration of the jet due to added buoyancy. The streamwise velocity profile also changes from a Gaussian to a flat-top Gaussian. The appearance of a twin-peak Gaussian profile for the temperature has been identified as the reason for this change in the streamwise velocity profile. The temperature profile changes to a flat-top Gaussian towards the end of the HIZ. These differences in the flow profiles are linked to the different decay rates of the axial velocity of heated and unheated jets. An empirical model incorporating the varying decay rates is also proposed.

1. Introduction

The current work is motivated by the desire to understand the effect of latent heat release in cumulus clouds. For this purpose we use a laboratory analogue consisting of a volumetrically heated jet. Professor Narasimha's group pioneered the use of such a model to study entrainment in cumulus clouds. The results from their experiments [1–3] provided important information about the behavior of volumetrically heated jets and plumes. These papers provide an excellent introduction to cloud entrainment in the presence of latent heat release, and the motivation for these experiments. Nevertheless, it is relevant to revisit details about entrainment by ordinary jets, and the interesting differences encountered in the presence of off-source heating.

Axisymmetric jets are examples of free-shear flows, and are driven by momentum supplied at the source. They spread by engulfing (entraining) the ambient fluid, such that their mass flux increases linearly with downstream distance while maintaining a constant momentum. Over the past few decades jets have established themselves as a preferred test-bed for experimental and numerical work. They are amongst the most popular flows on which new theories of turbulence are tested. Jet studies continue to provide valuable insights into complex phenomena such as mixing, combustion, aeroacoustics, propulsion and cloud formation. Their popularity can be gauged by the extensive literature that exists about them. Rajaratnam [4] and List [5] provide excellent reviews of jets.

* Corresponding author. Tel.: +1-302-831-2960; fax: +1-302-831-3619.
E-mail addresses: agrawaa@me.udel.edu (A. Agrawal), krs@jncasr.ac.in (K.R. Sreenivas), prasad@me.udel.edu (A.K. Prasad).
[1] Tel.: +91-80-846-2751; fax: +91-80-846-2766.

0017-9310/$ - see front matter © 2003 Elsevier Ltd. All rights reserved.
doi:10.1016/j.ijheatmasstransfer.2003.09.029

Nomenclature

A	multiplicative factor in equation for flat-top Gaussian velocity expression
B	flatness factor in equation for flat-top Gaussian velocity profile
b	local jet width
b'	nominal jet width corresponding to the mid-z location of the viewframe
B_u	decay rate constant of centerline velocity
c	lateral spread rate of the jet
C_p	specific heat
d	jet nozzle diameter
g	acceleration due to gravity
G	non-dimensional heating parameter
M	jet momentum
n	decay rate factor of centerline velocity in flat-top Gaussian velocity expression
Q	total power added to the jet
r	radial coordinate
Re	Reynolds number
Ri	Richardson number
U	streamwise velocity
U_c	jet centerline velocity
U_0	jet nozzle velocity
V	cross-stream velocity
z	streamwise coordinate
z_b	axial distance from nozzle where heating starts
z_0	axial location of virtual origin of jet

Greek symbols

α	coefficient of thermal expansion
μ	jet mass flux
ν	kinematic viscosity
ρ	density

Abbreviations

HIZ	heat injection zone
LIF	laser induced fluorescence
PIV	particle image velocimetry
TLC	thermochromic liquid crystals
CV	control volume

Morton et al. [6] first proposed that for free-shear flows in the self-similar regime, the mean entrainment velocity can be related to some characteristic velocity in the flow. The proportionality constant is called the coefficient of entrainment. A consequence of entrainment is that free-shear flows spread laterally into the ambient fluid at some characteristic angle. This model has been successfully applied to jets and plumes with and without density stratification and to several geophysical flows [7]. However, it has been found that the model of Morton et al. [6] is not strictly applicable for cumulus clouds which experience off-source buoyancy addition.

It is well known that lateral entrainment is almost non-existent in cumulus clouds [7–10]. Warner [8] shows that the standard lateral entrainment model for plumes cannot simultaneously predict the height of ascent and air–water ratio in cumulus clouds. If the air–water ratio is matched, then the ascent height is underpredicted, while matching the ascent height of the cloud results in too little dilution. Paluch [9] shows that the properties of air within cumulus clouds are attributable primarily to the mixing of air from below the cloud base with environmental air from near the cloud top, again attesting to the lack of lateral mixing. Emanuel [10] gives an excellent review of entrainment in cumulus clouds.

Clouds are rendered visible by condensed water vapor (water droplets) beyond the cloud base. The phase change is accompanied by latent heat release, and it is thought [1] that this added buoyancy significantly modifies the entrainment behavior of the rising plume. Consequently, cumulus clouds are generally characterized by vertical boundaries, i.e., they have almost no lateral spread (see photographs of cumulus clouds in Scorer [11]). The results reported here are the first in a series of experiments conducted at Delaware to understand the underlying mechanism for the reduced lateral entrainment in cumulus clouds due to latent heat release. We have chosen a laboratory analogue consisting of a turbulent axisymmetric jet to model a cumulus cloud. The jet fluid is selectively heated in an off-source manner to simulate condensation heat release above the cloud base (see [12] for details of the heating technique). The Richardson number, Ri (to be defined shortly) in our jet experiment is comparable to cumulus clouds, however, it is not possible to match the Reynolds number, Re for the two cases. Nevertheless, these experiments provide useful insights into the process of entrainment in cumulus clouds.

Bhat and Narasimha [1], and Elavarasan et al. [2] have replicated some of the features of clouds in a laboratory by adding off-source volumetric heat to an axisymmetric jet. [1] showed that the divergence angle of the jet reduces with off-source heating. For their investigation, $1600 \leqslant Re \leqslant 3200$, and the analogous heating parameter (to be defined shortly) $G \leqslant 5$. They found that coherent structures in the jet are disrupted by heat addition. They reported a drastic reduction in entrainment with heat addition. On the other hand, [2] measured an increase in mass flux of the jet in the heating

zone ($Re = 1360$, $Ri \leqslant 0.2$)—higher the heating rate, greater is the increase. However, in the post-heating zone, [2] reported a slightly smaller increment in the mass-flux with axial coordinate, as compared to normal jets.

Venkatakrishnan et al. [3] conducted off-source heating experiments in plumes ($Re = 2500$, $Ri = 0.26$) and also found a reduction in spread rate with heat addition. They reported higher and slightly lower entrainment rates towards the beginning and the end of the HIZ respectively. Venkatakrishnan et al. [13] investigated differences in heat addition on jets and plumes, and transition of jets to plumes in the post-heating zone. They found that plumes are more strongly affected by heat than jets, and the transition to plumes does not occur in the post-heating zone.

Sreenivas and Prasad [14] have argued that the vertical temperature gradient is the key parameter, and used it to explain the increase in entrainment rate with buoyancy addition at the source (plumes versus jets), in contrast to reduced entrainment with off-source buoyancy addition (volumetrically heated jets versus normal jets). Their model is based on the dynamics of the large engulfing vortices residing at the edges of jets and plumes (examples of large vortices residing at the edges of jets can be found in [15]).

Although Narasimha's group pioneered the effort to simulate latent heat release in cumulus clouds using a laboratory analogue, they were somewhat constrained by their use of laser doppler anemometry (LDA) to acquire velocity data. LDA is a point-wise technique implying that data must be collected on a suitable grid of measurement locations along the radial and axial coordinates. Measurements at each location must run for a long enough period to ensure reliable averages, and therefore, point-wise techniques are not ideally suited to an experiment whose runtime cannot exceed tens of minutes due to experimental conditions [1]. In contrast, PIV can provide hundreds of statistically uncorrelated frames over an extended planar domain with runtimes of just a few minutes. Each frame in turn provides streamwise and cross-stream velocity information at more than 3000 points on a two-dimensional grid. Note that existing results include only the streamwise component; second, these velocity profiles pertain mostly to the post-HIZ.

We have applied PIV and whole-field thermometry using thermochromic liquid crystals on volumetrically heated jets to better understand the role of off-source buoyancy addition on jets. The heating range for the present investigations is much larger and enables us to observe features which have not been previously reported. These include a flat-top Gaussian streamwise velocity profile, an inward cross-stream velocity profile, and, double-peaked and flat-top temperature profiles. Moreover, we found a relatively larger deceleration of the centerline velocity and a bulge in the velocity width at the beginning of the HIZ. These features (Reported for $G = 4.3$) have been revealed principally by our use of wholefield measurement techniques, although they are accentuated at larger heating rates.

This paper focuses on the axial and radial variation of the mean properties in the HIZ. It is shown that most of the underlying flow physics can be explained by examining just the mean quantities. The mean temperature rise can be related to the mean velocities through a model which we also propose. Consequently, we are able to uncover the complex coupling between velocity and temperature (which are in turn individually coupled to concentration) for this flow.

2. Experimental procedure

Our experimental setup and heat injection scheme are similar to those employed by [1,2]. Measurements were conducted in a 1.2 m tall glass tank with a 0.5 m square cross-section, which houses a nozzle at the bottom (orifice diameter, $d = 2$ mm). The jet was directed upwards and an axial plane of the jet was illuminated by laser light (Fig. 1). The viewframe was centered on the jet axis for all measurements reported in this paper. The jet fluid was volumetrically heated in an off-source manner using a scheme developed by Bhat et al. [12]. This method employs differences in water conductivity to selectively heat the jet fluid. Accordingly, the body of the jet was made conducting by adding hydrochloric acid to it (≈15 ml of HCl/l of jet water), whereas the ambient fluid in the tank was non-conducting deionized water. Densities of the jet and ambient water were

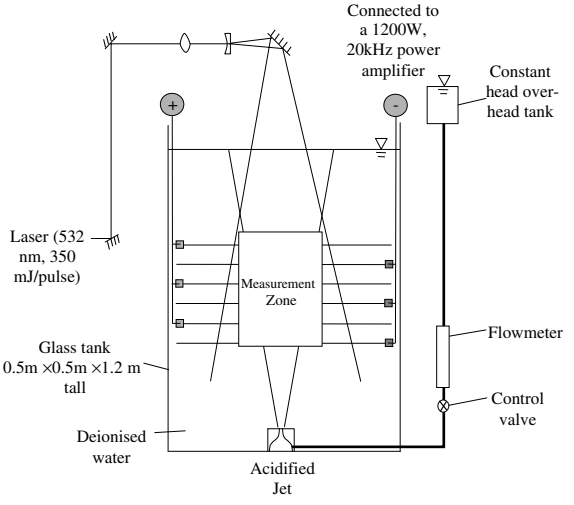

Fig. 1. Experimental setup.

matched by adding an appropriate amount of acetone to the jet fluid.

150 μm stainless steel wires spaced 1 cm apart on a square grid were used for heating the jet. Reynolds number based on wire diameter and the maximum velocity encountered at the grid location was less than 10, ensuring that vortex-shedding from the wires was not encountered (vortex-shedding can adversely affect the flow physics and is therefore undesirable). A copper bus bar supported each wire-mesh. The bus bar was "U" shaped (and not a complete rectangle) to minimize obstruction during LIF and PIV imaging.

For most of the measurements, we used 6 grids spaced 2.5 cm vertically. The alternate ones are connected to opposite terminals of a high power, high frequency power amplifier (1200 W at 20 kHz, Fig. 1). Such high frequencies were required to suppress electrolysis at the wires, which would otherwise subvert the supplied electrical power towards gas release (bubbles) instead of ohmic heating. When the jet was operating, only that portion of the jet body present between the multiple wire-grids conducted electricity resulting in ohmic heating, thus simulating latent heat release in clouds due to condensation. The power injected into the jet was calculated by monitoring the voltage and current across the grids. Note that power injection in the jet began only after it has attained stationarity.

Twin Nd-YAG pulsed lasers (350 mJ/pulse at 532 nm) provided illumination for PIV with a pulse separation of 36 ms. Beam-steering optics directed the light sheet downwards from the top of the tank to minimize obstructions from the copper bus bar. Images were recorded at 0.5 Hz using a Kodak 1.0 ES CCD camera with a 1026×1000 pixels array. 20–40 μm fluorescent particles were used as tracers for PIV. A long-wave filter was placed in front of the camera lens to block specular scattering (at 532 nm) from the grids while passing the fluorescent scattering from the particles. It was important to carefully optimize the particle concentration in the tank due to the large depth of viewing—small concentrations would adversely affect the interrogation of PIV images, whereas excessively large concentrations would severely attenuate the scattered light collected by the camera. The optimum value was obtained by gradually incrementing the concentration and evaluating PIV results.

The accuracy of our PIV technique is determined primarily by the error in locating the correlation peak to sub-pixel accuracy. Our estimated value is about 0.1 pixel, which is a typical value quoted by PIV practitioners [16]. In a typical run, the centerline velocity corresponds to a particle displacement of 6 pixels, therefore the error in the instantaneous velocity measurement is about $0.02U_c$.

Rhodamine 6G was used for LIF, and illumination was provided by the same lasers and sheet forming optics as for PIV. The long-wave filter was also employed during LIF imaging to reduce damaging specular reflections from the grids while passing fluorescence from the dye.

Temperature measurements were accomplished using 40 μm micro-encapsulated thermochromic liquid crystals (TLC) which serve as temperature sensors. See Smith et al. [17] for a review of the technique. The tank and jet fluids were seeded with TLCs to form a dilute suspension. A planar axial slice of the jet (coinciding with the PIV measurement plane) was illuminated with white light from slide projectors (two projectors were used to reduce shadowing effects). The wavelength of light that is preferentially scattered by the TLC depends on its temperature. Owing to its small size, the micro-encapsulated TLCs response time is a few milliseconds, implying that the temperature of the TLC corresponds closely to the fluid that carries it. A calibration look-up table was obtained by sequentially raising the temperature of the entire jet tank in small increments and recording the scattered color. We employed crystals with a 3.3 °C bandwidth (23.5–26.8 °C). TLC images were recorded at 2 Hz using a color CCD camera (DVC, with a 1300×1030 pixels array). The temperature results contribute significantly to our understanding of volumetrically heated jets.

The experimental results presented here are for different non-dimensional heating rates, and are compared against normal (unheated) jets. To quantify the effect of heat, the non-dimensional heating number, G [1] and Re are used as appropriate.

$$G = \frac{\alpha g}{\rho C_p}\frac{z_b^2}{d^3}\frac{Q}{U_0^3}, \quad Re = \frac{U_0 d}{\nu}, \tag{1}$$

where α is the coefficient of thermal expansion, g is acceleration due to gravity, ρ is the density of the unheated fluid, C_p is the specific heat, z_b is the axial distance from the nozzle where heating starts, d is the nozzle diameter, Q is the total power (W) added to the jet, U_0 is the nozzle exit velocity, and ν is the kinematic viscosity.

The Richardson number [2,3] is equivalent to G, and is expressed as

$$Ri = \frac{\alpha g}{\rho C_p}\frac{Q}{bU_c^3},$$

where b is the local jet width, and U_c is the local centerline velocity. b is defined as the radial location where the mean streamwise velocity is e^{-1} of the mean centerline velocity U_c. Ri and G are related as

$$Ri = G\frac{d^3}{z_b^2 b}\frac{U_0^3}{U_c^3}.$$

Therefore, $G = 12.5\,Ri$.

3. Results and discussion

3.1. Unheated jet (baseline)

A set of baseline experiments was carried out to characterize the normal (unheated) jet flow, and to check if the flow was affected by the presence of the grids. Both LIF and PIV results were virtually identical with and without grids, confirming that the grids did not affect the flow. Next, values of important baseline parameters of the jet were obtained by PIV measurements without the grids for $Re = 3000$ and $110 \leqslant z/d \leqslant 175$. The unnormalized and normalized streamwise velocity profiles for these measurements are shown in Fig. 2a and b. Fig. 2a shows that the velocity at each downstream location is Gaussian in nature. The centerline velocity, $U_c \sim z^{-1}$, while the jet width $b \sim z$ in agreement with standard results for axisymmetric jets.

A standard normalization procedure is employed in Fig. 2b—the streamwise velocity, U is normalized by U_c, and the radial coordinate r by the local jet width, b. According to the usual definitions for axisymmetric jets,

$$U_c = \frac{U_0 B_u d}{(z - z_0)}$$

and $b = c(z - z_0)$, where B_u specifies the decay rate of the time-averaged centerline velocity, c is the lateral spread rate, z is the axial coordinate, and z_0 is the virtual origin of the jet. The values of B_u, c and z_0/d were obtained by a least squares fit to the data as 4.7, 0.11, and 4, respectively. Our values closely match the values generally quoted in literature [18] (see also Fischer et al. [19] for the range of c). The collapse upon normalization (Fig. 2b) further confirms that the jet has achieved self-similarity at this downstream location (deviation from the mean amounting to ±3% at the centerline is largely due to experimental scatter). Self-similarity was confirmed at all axial locations before commencing detailed measurements.

The measured cross-stream velocity, V normalized by U_c, along with the theoretical profile obtained by integrating the continuity equation (assuming a Gaussian streamwise velocity profile) are plotted in Fig. 3. The cross-stream component of the velocity is small (maximum of ≈2% of the local mean centerline velocity). In fact, the corresponding particle displacement is only 0.1 pixel which is on the order of the least count of our measurement technique. Therefore, the scatter associated with these measurements is rather large. Nevertheless the mean value is in good agreement with the theoretical profile for $r/b < 1.5$. The deviation at larger r/b could be due to the finite size of the tank, or the small difference between the measured streamwise

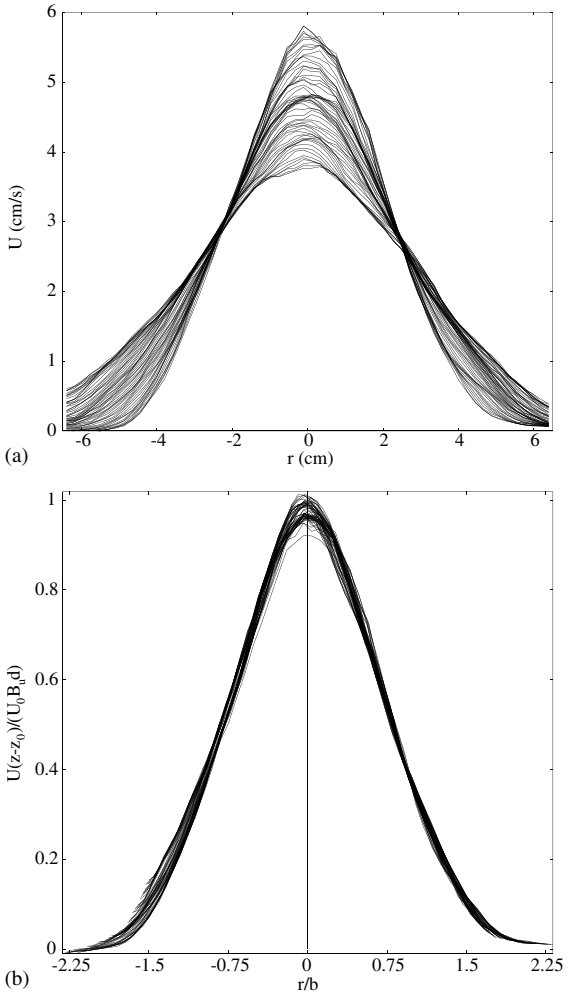

Fig. 2. (a) Unnormalized and (b) normalized streamwise velocity profile ($Re = 3000$, $110 \leqslant z/d \leqslant 175$).

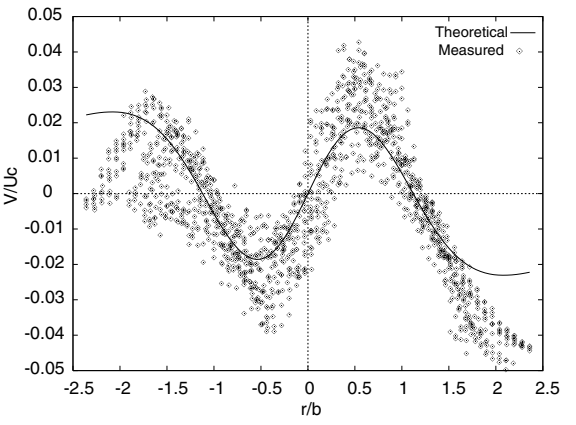

Fig. 3. Measured versus theoretical cross-stream velocity profiles ($Re = 3000$, $110 \leqslant z/d \leqslant 175$).

velocity profile and the fitted Gaussian function. It should be noted that V changes sign around $r/b = 1.1$, indicating that the jet experiences an outflow near the time-averaged jet-axis and an inflow far away from it. The decay in the centerline velocity with downstream distance is associated with a decrease in the axial volume flux for a small control volume (CV) centered at the axis [21]. The excess volume exits the lateral sides of the CV resulting in a lateral outflow near the jet-axis. However, for a CV extending to large r/b and therefore encompassing almost the entire jet, a net increase in the axial volume flux is associated with a radially inwards pointing lateral volume flux.

3.2. Volumetrically heated jet

3.2.1. Visualization results

Instantaneous LIF images in Fig. 4a and b (without and with heat injection, respectively) confirm the dramatic effect of heat addition on the jet ($Re = 2000$, $G = 1$) that was first reported by [2]. Likewise, the presence of large eddies is less evident in the heated jet. (Bright horizontal lines in the viewframe indicate location of the grids, while dark vertical lines are shadows from the wires. The grid spacing in Figs. 4 and 5 is 5 cm.) Time-averaged (of 48) LIF images in Fig. 5a and b (without and with heat injection, respectively) clearly show a reduction in spread rate with heat addition. Our LIF results therefore confirm the earlier findings of [1–3]. Because scalar measurements have been adequately discussed in Bhat and Narasimha [1], we do not elaborate on these results here.

Further evidence of the effect of heat addition is obtained by visualization with liquid crystals. More information can be gleaned from TLC frames as compared to LIF, because unlike the dye, these crystals are present both in the jet and the ambient fluid. The differences in color further provide an indication of the amount of mixing of the ambient and jet fluids. Fig. 6 is an example of a TLC image ($Re = 1450$, $202 \leqslant z/d \leqslant 267$, $G = 13.5$). The ambient is at 23.5 °C (red), while the jet fluid changes from the ambient color near the bottom of the frame to blue near the top. This indicates that initially the jet is at the ambient temperature (as expected), and the temperature increases with the axial coordinate due to heat addition. The sharp demarcation of colors at the jet boundary, along with almost no change in color of the ambient fluid, indicates that the jet fluid is indeed getting selectively heated. One can make three important observations by comparing the jet before the second grid (in the frame) versus the jet downstream of this grid location: (1) the narrowing of the jet is apparent beyond the second grid; (2) large eddies are observed upto this axial location and are less apparent beyond it indicating that eddies are disrupted *only* in the latter part of the HIZ; (3) the jet appears to be getting axially stretched beyond the second grid. Bhat and Narasimha [1] reported a subsequent reduction in the scalar width in agreement with our first observation.

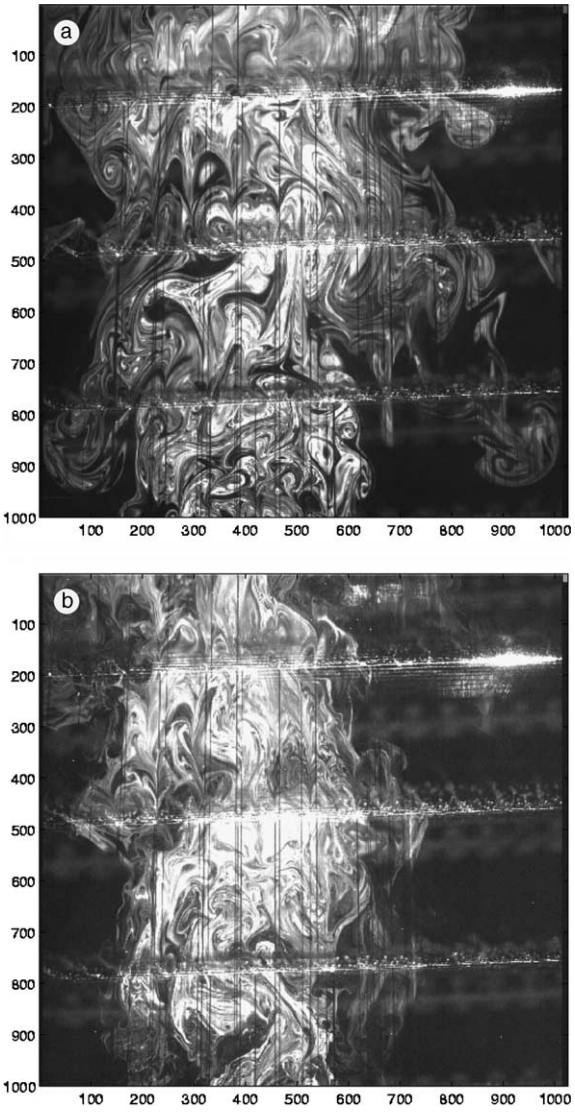

Fig. 4. Instantaneous LIF visualization: (a) without and (b) with heat addition ($Re = 2000$, $G = 1$).

While previous studies reported that large eddies are disrupted with heat injection, our results indicate that this disruption occurs only in the latter part of the HIZ. (See [20] for quantitative evidence for the disruption of eddies in the latter part of the HIZ.) Such a delayed disruption of large eddies suggests that heat requires a finite time to act and disrupt the coherent structures in the flow. The coupling between disruption of eddies and reduction in the jet spread rate is also discussed in [20]. Disruption of the large eddies might partly be the reason for the observed decrease in the spread rate.

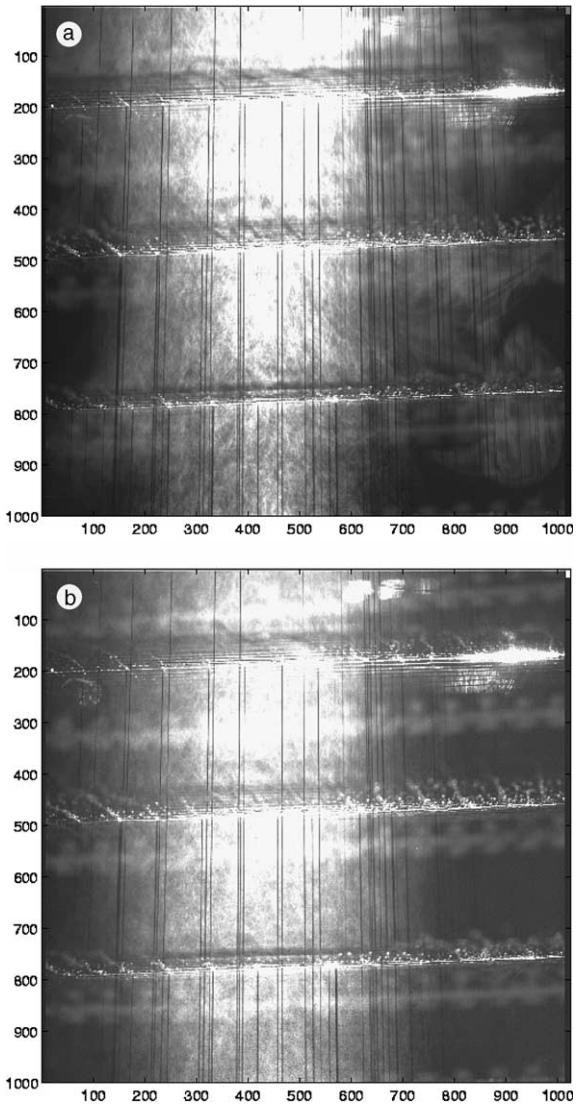

Fig. 5. Average of 48 LIF visualizations: (a) without and (b) with heat addition ($Re = 2000$, $G = 1$).

3.2.2. Velocity measurements

The HIZ extends between $200 \leqslant z/d \leqslant 265$ for PIV measurements. The extent of the HIZ is chosen such that its height is 2–3 times the nominal jet width. In other words, we tried to maintain a similar height to width ratio as employed by [1] and found in cumulus clouds. The viewframe corresponding to $200 \leqslant z/d \leqslant 289$ includes and extends slightly beyond the HIZ. Bhat and Narasimha [1] have already shown that the behavior of the jet in the pre-heating zone resembles a normal jet, and that eddies reappear 3–4 jet widths downstream of the HIZ. Our viewframe therefore focuses on the region affected most severely by heat injection.

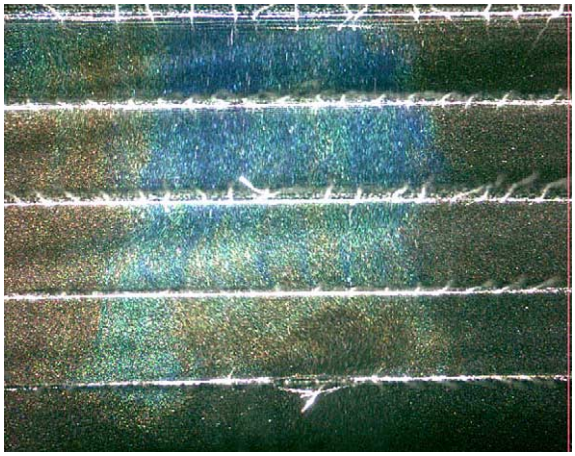

Fig. 6. Temperature visualization in a heated jet (red = cold, blue = hot; $Re = 1450$, $G = 13.5$).

Along the lines of the temperature visualizations described above, it is possible to identify three distinct regions located axially in the heated zone. We have used the cross-stream velocity profiles to demarcate these three regions. As mentioned earlier, the cross-stream velocity, which is the key indicator for the different zones has not been previously measured. The streamwise and cross-stream velocity profiles from an average of 337 statistically independent frames for the three regions are presented in Figs. 7 and 8, respectively.

The lower zone (zone-1) barely shows any effect of heat on the jet—the streamwise velocity is still Gaussian in nature (Fig. 7), and the cross-stream velocity profile exhibits an outflow for small r, and there is a tendency towards an inflow at large r (Fig. 8) that closely resembles the baseline, unheated case.

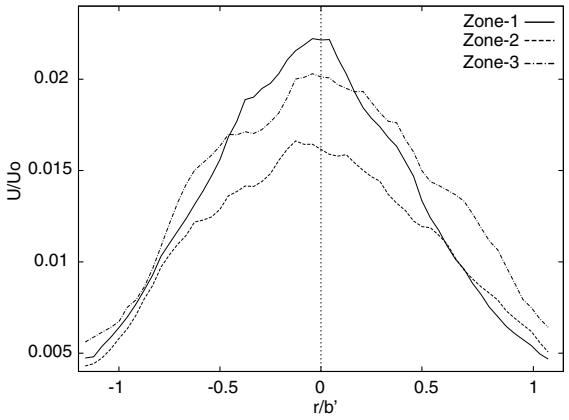

Fig. 7. Streamwise velocity profiles for different zones ($Re = 2400$, $G = 4.3$, b' is the nominal jet width corresponding to the mid-z location of the viewframe).

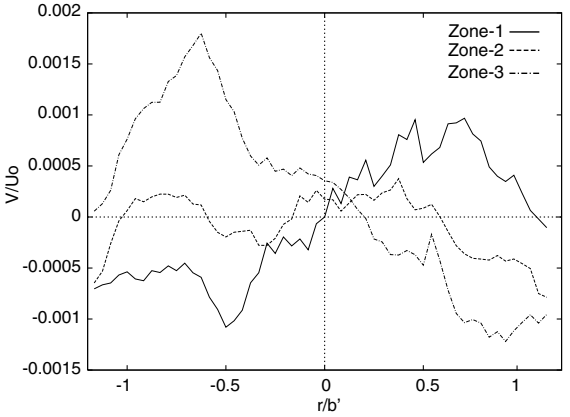

Fig. 8. Cross-stream velocity profiles for different zones ($Re = 2400$, $G = 4.3$).

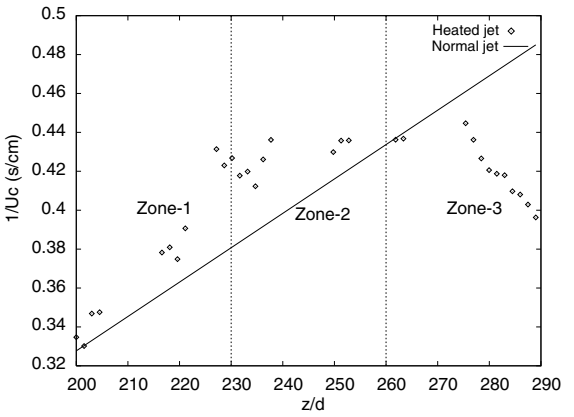

Fig. 9. Centerline velocity for normal and heated jets ($Re = 2400$, $G = 4.3$).

The middle zone (zone-2) exhibits a change in the cross-stream velocity profile. The streamwise velocity is in a transitional state between zones 1 and 3 (Fig. 7), and the cross-stream velocity is nearly zero for all r in the viewing zone (Fig. 8). Despite large fluctuations in the V profile, the mean can be seen to be nearly zero, i.e., in contrast to unheated jets, regions of mass influx or outflux are not observed for the radial extent covered by the viewframe (Fig. 8).

The upper zone (zone-3) shows a strong effect of heating on the jet: the streamwise velocity profile changes from a Gaussian to a flat-top Gaussian profile (Fig. 7). The cross-stream velocity profile shows a remarkable deviation from a normal jet profile in this zone. As can be readily seen from Fig. 8, the cross-stream velocity, V is inward for small r and tends to 0 further out, i.e., a mass inflow is seen for all r in this zone. Note that V cannot turn positive for r beyond the viewframe, as that would violate continuity.

Fig. 9 presents the variation of U_c with z for a heated jet versus an unheated axisymmetric jet. ($1/U_c$ is plotted for an easier comparison with the unheated jet.) It is seen that $1/U_c$ increases a little and then decreases. The decrease in U_c indicates deceleration and corresponds to a slightly wider than normal jet (as shown below); however, as heat starts to affect the jet, the decay of U_c is arrested (zone-2). Finally, due to the cumulative effect of heat addition the jet starts to accelerate (zone-3). Bhat and Narasimha [1] have also observed a slight acceleration of the jet at the end of the HIZ and the beginning of the post-HIZ, but they did not report the excess deceleration at the beginning of the HIZ. A slightly larger relative deceleration at the beginning of the HIZ can be discerned in Fig. 4 of Venkatakrishnan et al. [3].

The coupling between centerline velocity decay rate and volume outflow can be understood in the following simple way [21]. First, let us obtain the cross-stream velocity profile, V/U_c for axisymmetric and planar jets and plumes by integrating the continuity equation assuming a Gaussian streamwise velocity profile. Next, one can determine the radial location (or a cross-stream location for planar jet and plume) where the V/U_c profile experiences a zero-crossing, i.e., where a change-over from outflow to inflow occurs. The above exercise yields an interesting result which is summarized as follows. The decay rates of axisymmetric jets, planar jets, and axisymmetric plumes are respectively z^{-1}, $z^{-1/2}$, $z^{-1/3}$, while the radial extents of outflow are $r/b \leqslant 1.12, 0.99, 0.59$. Moreover, the decay rate for planar plumes varies as z^0 and these do not experience any outflow. Two interesting observations can now be made. First, the decay of the centerline velocity is responsible for an outflow, and second, a higher decay rate correlates with a larger radial extent of outflow. Although the above examples pertain to different configurations of free-shear flows, a similar argument suggests that a decrease in the decay rate should lead to a smaller radial extent of outflow for the volumetrically heated jet as well. Eventually an accelerating jet will experience a pure inflow towards the jet axis for all r. Therefore, the results of Figs. 8 and 9 are consistent with the results obtained from the exercise suggested here.

The velocity width of the jet as a function of the downstream coordinate is plotted in Fig. 10. The result is in *contrast* with the scalar width result—the velocity width for the heated jet is larger than the unheated jet. Moreover, the velocity width of the jet increases in the initial part of the HIZ, and then remains constant or decreases with z. Bhat and Narasimha [1] allude to this result although on the basis of only three data points (within, at the end, and beyond the HIZ). The increase in velocity width over-and-above that for a normal jet during the initial part of the heating zone is expected, because momentum which varies as $b^2U_c^2$ (assuming a

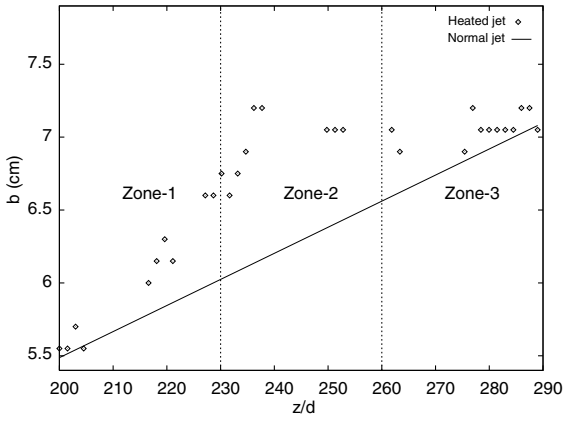

Fig. 10. Velocity widths for normal and heated jets ($Re = 2400$, $G = 4.3$).

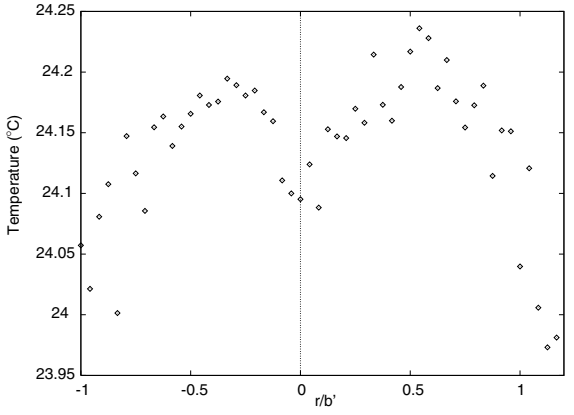

Fig. 11. Time-averaged temperature for $241 \leqslant z/d \leqslant 245$ ($Re = 1450$, $G = 13.5$).

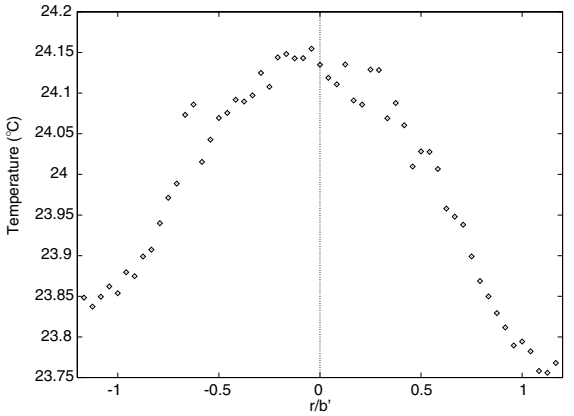

Fig. 12. Time-averaged temperature for $257 \leqslant z/d \leqslant 263$ ($Re = 1450$, $G = 13.5$).

Gaussian profile in zone-1) must increase with z due to heat addition, whereas U_c is seen to decrease faster than z^{-1} (Fig. 9). The subsequent decrease in velocity width might be linked to a decrease in the scalar distribution width (note that the volumetric heat addition is directly proportional to the local acid concentration).

3.2.3. Temperature measurements

Referring back to the TLC frame in Fig. 6, it can be seen that for an axial location upstream of the fourth grid, the temperature increases with r and then decreases. This can be explained in the following way: for a Gaussian velocity and scalar distribution, the fluid near the centerline carries the most acid but has the least residence time in the HIZ; similarly, the fluid at the jet edge has the largest residence time but the smallest acid concentration. Now, the temperature rise increases with residence time, and the rate of heat injection. Because the rate of heat injection is proportional to the acid concentration, the two opposing effects could produce a temperature rise whose maximum lies away from the centerline. This observation is confirmed by time-averaging the individual temperature fields between the third and fourth grids (Fig. 11, $241 \leqslant z/d \leqslant 245$). Although the average (of 172 frames) maximum temperature rise is small (less than 1 °C) the twin peaks can be clearly discerned. (While the scatter in the temperature profile is at most 0.02 °C, the dip at the centerline is about 0.08 °C indicating that the double-peaked profile is genuine. Our DNS [22] has provided additional confirmation for this result.) Bhat and Narasimha [1] also conjectured that a given temperature rise has a more pronounced effect towards the edge of the jet than near the axis.

The time-averaged temperature between the last two grids ($257 \leqslant z/d \leqslant 263$) is shown in Fig. 12. At this location, the temperature profile has evolved further and resembles a flat-top Gaussian. The evolution of temperature profiles between the two axial locations (Figs. 11 and 12) could be linked to the evolution of velocity profiles from a Gaussian in zone-2 to a flat-top Gaussian in zone-3. This is explained as follows: for a flat-top Gaussian velocity profile the residence time in the HIZ is almost the same for fluid in a substantial neighborhood around the centerline. Assuming a flat-top Gaussian distribution for acid concentration [23,24], the temperature rise will be nearly uniform near the centerline, resulting in a flat-top Gaussian profile for temperature.

3.2.4. Variation in heating rates

The heating parameter G encapsulates the relative effect of heat injection on the turbulent jet. As indicated in Eq. (1), G can be increased by either decreasing Re, working farther from the nozzle, or, by increasing the rate of heat injection Q into the jet (Q can be increased by either adding more acid to the jet fluid, or by

applying a higher voltage across the grids). $0 \leqslant G \leqslant 14$ has been employed in the present investigation.

The jet passes through the heating zone almost unaffected for small values of G. However as G increases, the spread rate decreases. The jet rises like a column and even converges (instead of diverging) for still higher values of G. These observations are consistent with those of [1].

Moreover, we found that with higher G, the second and third zones move closer to z_b, the axial location where heat is first injected into the jet. This is expected because the jet feels the effect of heat more strongly as G increases. Based on the evidence, we can conjecture the existence of a critical temperature beyond which the transition (sudden change in spread rate) occurs. The transition from a pure Gaussian to a flat-top Gaussian (in zone-3) is not apparent for lower G, however, as G increases the flat top becomes more pronounced. Further, the radial extent of the flat top region increases with larger G. Nevertheless, similar qualitative trends apply for the entire range of G investigated herein.

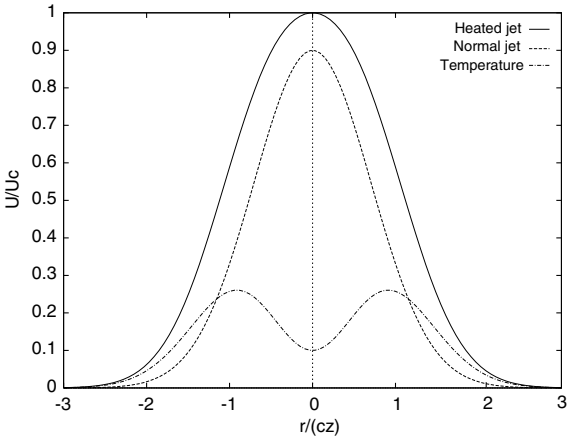

Fig. 13. Effect of volumetric heat injection on the streamwise velocity. The heated jet profile corresponds to Eq. (2). The double-peaked temperature profile is obtained by subtracting the Gaussian (normal jet) profile of a smaller magnitude from the flat-top Gaussian profile.

3.3. Empirical model for the heated jet

The flat-top Gaussian streamwise velocity profile for the heated jet (in zones-2 and -3) can be well represented by

$$U = \frac{AU_0}{z^n}\left(1 + \frac{Br^2}{c^2z^2}\right)\exp\left(-\frac{r^2}{c^2z^2}\right), \tag{2}$$

where n characterizes the decay rate of the centerline velocity, B is the flatness factor for the flat-top Gaussian (flatness increases with B), and A is a factor that enforces dimensional homogeneity. It should be noted that ($B = 0$, $n = 1$) returns a Gaussian profile (normal jet). Heat injection causes the velocity to decay less rapidly, i.e., makes $n < 1$, and distorts the Gaussian to a flat-top Gaussian ($B > 0$). We expect $B \leqslant 1$, because $B > 1$ produces a velocity double-peak which is not observed experimentally. Thus, while n reflects the axial effect of heating, B captures the radial effect of heating.

Eq. (2) allows further interesting insights by a simple manipulation. If a Gaussian (of slightly reduced height) is subtracted from Eq. (2) the resulting profile exhibits twin peaks, and resembles the temperature profile in Fig. 11 quite closely (Fig. 13). The implication is that, the flat-top Gaussian is a superposition of a Gaussian profile and a twin-peak profile. It may be argued that a twin-peak temperature profile (Fig. 11) corresponding to a twin-peaked buoyancy addition will lead to a twin-peaked velocity perturbation that is superposed on the original Gaussian velocity profile. Thus, it is plausible that the observed temperature distribution is responsible for transforming the original Gaussian velocity profile to a flat-top Gaussian. This flat-top velocity profile could in turn change the twin peak Gaussian for temperature (at $z/d = 243$) to a flat-top (at $z/d = 260$) as conjectured in the previous section.

The continuity equation with a substitution for U according to Eq. (2) can be integrated to yield the cross-stream velocity, V for the volumetrically heated jet. Results for ($B = 0$, $n = 1$), ($B = 1/2$, $n = 0$) and ($B = 2/3$, $n = -1/2$) are plotted in Fig. 14. The first of these three cases corresponds to a normal jet, and the V profile indicates an outflow for $r/b \leqslant 1.1$ before undergoing a zero-crossing and becoming an inflow for larger r/b. The second case corresponds to a centerline velocity that is neither increasing nor decreasing with $z(n = 0)$, therefore there is neither an inflow nor an outflow near

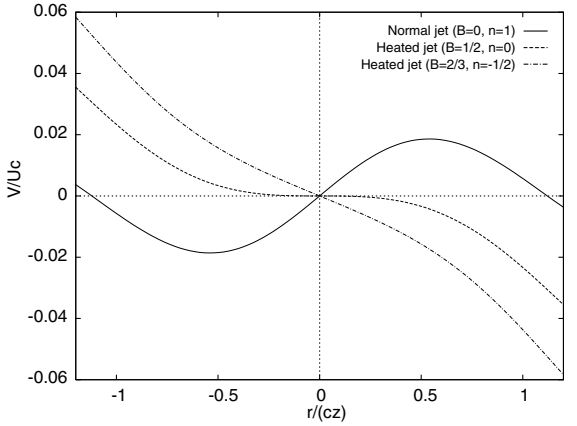

Fig. 14. Effect of volumetric heat injection on the cross-stream velocity derived from the empirical model.

the centerline. The third case corresponds to an accelerating centerline velocity, therefore the V velocity indicates an inflow for all r/b. These profiles capture the trend of the cross-stream velocity profile in Fig. 8 quite well: the profile for zones 1, 2, and 3 (Fig. 8) are respectively similar to the three cases outlined here (Fig. 14). In particular, data for zone 3 in Fig. 8 matches very well with the cross-stream profile corresponding to ($B = 0.2$, $n = -1/2$).

The ratio of momentum corresponding to an axisymmetric jet with the velocity profile given by Eq. (2) to a normal jet, is given by

$$\frac{M_{\text{heat}}}{M_{\text{normal}}} = \frac{1 + (1+B)^2}{2}. \tag{3}$$

Eq. (3) assumes that both profiles have identical jet widths and centerline velocities. For this situation, Eq. (3) provides the expected result that the momentum transported by the heated jet profile is larger than for a jet with a Gaussian velocity profile. This might partly explain the change from Gaussian to a flat-top Gaussian with heating.

Similarly, for the same centerline velocity and jet width, the ratio of the mass fluxes for the heated versus a normal jet can be obtained as

$$\frac{\mu_{\text{heat}}}{\mu_{\text{normal}}} = 1 + B, \tag{4}$$

i.e., the mass flux for a heated jet is $(1 + B)$ times larger than a normal jet. The results in Eqs. (3) and (4) should be interpreted keeping in mind the assumption of the same jet width and centerline velocity. Nevertheless, they provide a simple and useful way to compare the momentum and mass fluxes of the heated and normal jets without additional complicating factors.

4. Conclusions

Off-source volumetric heat was added to an axisymmetric turbulent jet to simulate the latent heat release effect in cumulus clouds. Although the experimental setup is similar to Bhat and Narasimha [1], the current application of wholefield velocimetry and thermometry has allowed us to probe in detail the velocity and temperature fields *within* the heat injection zone (HIZ) for the first time, leading to several new and unexpected results. While our results have confirmed certain previously reported observations such as a reduction in scalar width and the disruption of large eddies [1], we found a flat-top Gaussian streamwise velocity profile, an inward cross-stream velocity profile, and double-peaked and flat-top temperature profiles. Moreover, we found a relatively larger deceleration of the centerline velocity and a bulge in the velocity width at the beginning of the HIZ. In addition, the large eddies are seen to be disrupted by heating in the latter part of the HIZ, and this results in an eventual reduction of the scalar and velocity widths. We have also measured the cross-stream velocity and temperature profiles for the first time, and elucidated the complex interplay of concentration, temperature and velocity fields for this flow.

The decay rate for the jet in the initial part of the HIZ is slightly larger than normal jets, but subsequently the centerline velocity increases. The initial increase in decay rate corresponds to a slightly wider than normal jet. However, heat injection causes a subsequent increase in the centerline velocity as was also reported in [1]. An increase in the average centerline velocity is responsible for an inflow for all radial locations in the viewframe.

A substantial change in the cross-stream velocity is noted while moving downstream through the HIZ. The difference in behavior is employed to demarcate the HIZ into three sub-zones. In zone-1, the effect of heat on the shape of the velocity profiles is barely noticeable. In zone-2, the decay of the centerline velocity is arrested, and the cross-stream velocity is nearly zero for all radial positions in our viewfield. In zone-3, acceleration of the jet strongly affects both the velocity components. The Gaussian is distorted to a flat-top Gaussian, while an inward velocity is observed for all radial locations. Large eddy structures are seen only till zone-1, beyond which they are disrupted by heating. The axial location of these zones vary with the amount of heat added to the jet.

The time-averaged temperature profile exhibits a double-peak in zone-2, and resembles a flat-top Gaussian in zone-3. We provide an explanation for this interesting observation through physical arguments, and also through a model. Our proposed model is consistent with the observed velocity profiles of U and V, and (expectedly) predicts an increase in momentum flux with heat addition. The model further predicts a larger mass flux for the heated jet compared to their unheated counterparts assuming the same velocity width for the two cases. This empirical model has been extended to entrainment in cumulus clouds [24].

Acknowledgements

This work was supported by National Science Foundation, under grants NSF-ATM-9714810 and 0095122.

References

[1] G.S. Bhat, R. Narasimha, A volumetrically heated jet: large eddy structure and entrainment characteristics, J. Fluid Mech. 325 (1996) 303–330.

[2] R. Elavarasan, G.S. Bhat, R. Narasimha, A. Prabhu, An experimental study of a jet with local buoyancy enhancement, Fluid Dyn. Res. 16 (1995) 189–202.

[3] L. Venkatakrishnan, G.S. Bhat, R. Narasimha, Experiments on a plume with off-source heating: implications for cloud fluid dynamics, J. Geophys. Res. 104 (1999) 14271–14281.
[4] N. Rajaratnam, Turbulent Jets, Elsevier Science, 1976.
[5] E.J. List, Turbulent jets and plumes, Ann. Rev. Fluid Mech. 14 (1982) 189–212.
[6] B.R. Morton, G.I. Taylor, J.S. Turner, Turbulent gravitational convection from maintained and instantaneous sources, Proc. R. Soc. London A 234 (1956) 1–23.
[7] J.S. Turner, Turbulent entrainment: the development of the entrainment assumption, and its application to geophysical flows, J. Fluid Mech. 173 (1986) 431–471.
[8] J. Warner, On steady-state one-dimensional models of cumulus convections, J. Atmos. Sci. 27 (1970) 1035–1040.
[9] I.R. Paluch, The entrainment mechanism in Colorado cumuli, J. Atmos. Sci. 36 (1979) 2467–2478.
[10] K.A. Emanuel, Atmospheric Convection, Oxford University Press, 1994.
[11] R. Scorer, Clouds of the World—A Complete Color Encyclopedia, Lothian Pub. Co, 1972.
[12] G.S. Bhat, R. Narasimha, V.H. Arakeri, A new method of producing local enhancement of buoyancy in liquid flows, Exp. Fluids 7 (1989) 99–102.
[13] L. Venkatakrishnan, G.S. Bhat, A. Prabhu, R. Narasimha, Visualization studies of cloud-like flows, Curr. Sci. 74 (1998) 597–606.
[14] K.R. Sreenivas, A.K. Prasad, Vortex-dynamics model for entrainment in jets and plumes, Phys. Fluids 12 (2000) 2101–2107.
[15] A. Agrawal, A.K. Prasad, Organizational modes of large-scale vortices in an axisymmetric turbulent jet, Flow Turbul. Combust. 68 (2002) 359–377.
[16] A.K. Prasad, Particle image velocimetry, Curr. Sci. 79 (2000) 101–110.
[17] C.R. Smith, D.R. Sabatino, T.J. Praisner, Temperature sensing with thermoclinic liquid crystals, Exp. Fluids 30 (2001) 190–201.
[18] I. Wygnanski, H. Fiedler, Some measurements in a self-preserving jet, J. Fluid Mech. 38 (1969) 577–612.
[19] H.B. Fischer, E.J. List, R.C.Y. Koh, J. Imberger, N.H. Brooks, Mixing in Inland and Coastal Waters, Academic Press, 1979.
[20] A. Agrawal, A.K. Prasad, Evolution of a turbulent jet subjected to volumetric heating, J. Fluid Mech., in review.
[21] A. Agrawal, A.K. Prasad, Integral solution for the mean flow profiles of turbulent jets, plumes and wakes, J. Fluids Eng. 125 (2003) 813–822.
[22] A. Agrawal, B.J. Boersma, A.K. Prasad, Direct numerical simulation of a turbulent axisymmetric jet with buoyancy induced acceleration, Flow Turbul. Combust., in review.
[23] R. Narasimha, V. Saxena, S.V. Kailas, Coherent structures in plumes with and without off-source heating using wavelet analysis of flow imagery, Exp. Fluids 33 (2002) 196–201.
[24] A. Agrawal, Effect of off-source volumetric heat addition on entrainment in a turbulent jet with application to cumulus clouds, Ph.D. dissertation, University of Delaware, 2002.